JACS
JOURNAL OF THE AMERICAN CHEMICAL SOCIETY
Article
pubs.acs.org/JACS

Particle Formation during Oxidation Catalysis with Cp* Iridium Complexes

Ulrich Hintermair,[†] Sara M. Hashmi,[§] Menachem Elimelech,*[,§] and Robert H. Crabtree*[,†]

[§]Department of Chemical and Environmental Engineering, Yale University, 9 Hillhouse Avenue, New Haven, Connecticut 06520, United States

[†]Department of Chemistry, Yale University, 225 Prospect Street, New Haven, Connecticut 06520, United States

Supporting Information

ABSTRACT: Real-time monitoring of light scattering and UV−vis profiles of four different Cp*Ir^{III} precursors under various conditions give insight into nanoparticle formation during oxidation catalysis with $NaIO_4$ as primary oxidant. Complexes bearing chelate ligands such as 2,2′-bipyridine, 2-phenylpyridine, or 2-(2′-pyridyl)-2-propanolate were found to be highly resistant toward particle formation, and oxidation catalysis with these compounds is thus believed to be molecular in nature under our conditions. Even with the less stable hydroxo/aqua complex $[Cp^*_2Ir_2(\mu\text{-}OH)_3]OH$, nanoparticle formation strongly depended on the exact conditions and elapsed time. Test experiments on the isolated particles and comparison of UV−vis data with light scattering profiles revealed that the formation of a deep purple-blue color (∼580 nm) is *not* indicative of particle formation during oxidation catalysis with molecular iridium precursors as suggested previously.

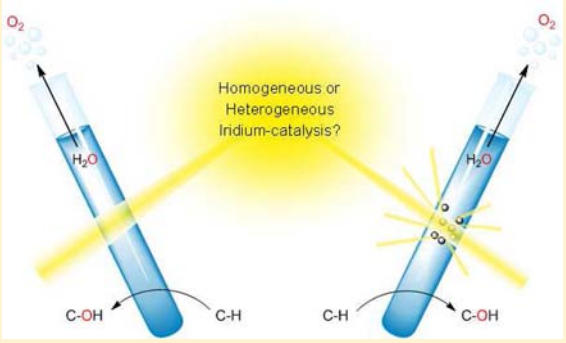

INTRODUCTION

Half-sandwich Cp*Ir^{III} complexes (Cp* = pentamethylcyclopentadienyl) are efficient precursors for stereoretentive C−H[1,2] hydroxylation and water[3−8] oxidation catalysis. These reactions constitute key steps for the realization of alternative energy conversion schemes,[9−12] the upgrading of unreactive feedstocks,[13−16] and the development of new synthetic methodologies.[17−19] Investigation of the active catalyst species is thus of great interest and is expected to yield significant improvements based on mechanistic understanding. Unfortunately, the strongly oxidizing conditions required to drive these reactions complicate studying the catalyst at work and raise concerns about homogeneity, a persistent ambiguity in organometallic catalysis research.[20] A number of tests probing the formation of metal nanoparticles have been developed for reductive catalysis with transition metal complexes,[20,21] but far fewer methods are available for oxidation catalysis.[22] We recently described the application of a highly sensitive electrochemical quartz crystal nanobalance (EQCN) technique to distinguish homogeneous from heterogeneous catalysis with Cp*Ir^{III} complexes in electrode-driven water oxidation.[23] We now present time-resolved dynamic light scattering (DLS) as a powerful tool to gain insight into particle formation during oxidation catalysis with organometallic iridium complexes using chemical oxidants.

Just as metal clusters may easily form under reducing conditions, the formation of metal oxide particles is not surprising when organometallic transition metal complexes are subjected to strongly oxidizing conditions. To understand the true origin of the catalysis, however, we need to know the kinetic stability of the molecular precursor and the rate of particle formation under the conditions applied in order to assess the potential involvement of the heterogeneous material in the reaction. Electron microscopy on an aliquot taken at the end of the reaction is often used to check for particles, but such post operandum analysis does not necessarily apply to the catalytic reaction itself since changes may occur during the required pretreatment of the sample and even under the electron beam irradiation needed for the measurement.[20] Time-resolved dynamic light scattering (DLS) is a powerful technique for investigating the formation and growth dynamics of solid particles in solution,[24] and has the great advantage of being directly applicable to working catalyst solutions. Technical advances in the instrumentation mean that modern correlators easily reach temporal resolution on the order of microseconds, giving nanometer-scale particle detection limits in aqueous solutions.[25−27]

Oxidation catalysis with molecular iridium compounds is particularly delicate because of the high catalytic activity of iridium oxides[28−30] potentially forming in situ from an organometallic precursor. While the exceptional reactivity of iridium oxides can be exploited for robust and practical heterogeneous catalysts in various contexts, this instability bedevils the study and development of homogeneous Ir-based oxidation catalysts. Not only is the detection of finely dispersed metal-oxide material difficult, but the chemistry of iridium

Received: April 5, 2012
Published: May 17, 2012

dx.doi.org/10.1021/ja3033026 | J. Am. Chem. Soc. 2012, 134, 9785−9795

Scheme 1. The Formation of Purple-Blue Solutions of Ir^{IV}

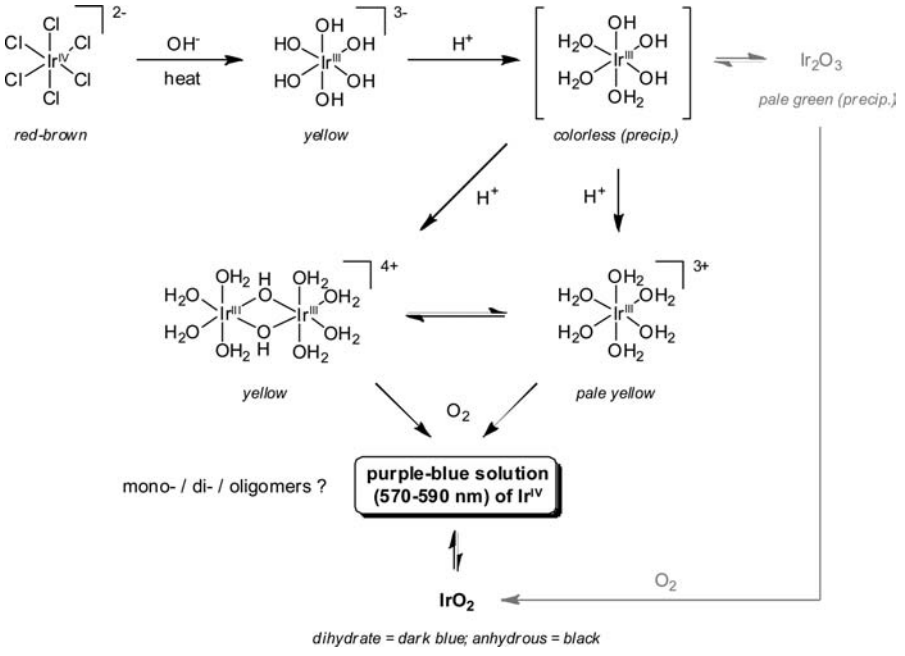

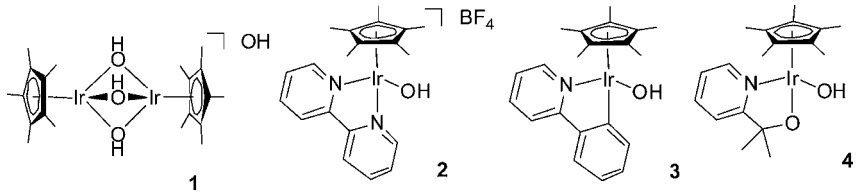

Figure 1. The Cp^*Ir^{III} complexes investigated.

oxides itself remains somewhat problematic, even after two centuries of research.[31−33] Since the early work of Wöhler,[34] the appearance of a deep purple-blue color with an intense, broad UV−vis absorption having a λ_{max} around 570−590 nm has often been associated with colloidal IrO_2 in solution. Harriman showed that such blue solutions formed by hydrolysis of hexachloroiridate may contain amorphous IrO_2 particles of 4 nm diameter which aggregate to larger clusters ∼100 nm in size.[35] He also demonstrated that these materials are good water oxidation catalysts,[29,36] and IrO_2 nanoparticles synthesized via this route have since then been used as oxidation catalysts in various systems.[37−44] Catalyst formation is typically monitored by the appearance of the broad ∼580 nm UV−vis absorption, and irradiation in this spectral regime has even been investigated as energy input for light-driven water oxidation.[45] However, this UV−vis band cannot be securely identified as a surface plasmon resonance because it often arises from d−d transitions of distorted octahedral Ir^{IV} centers,[46] and is thus not per se indicative for heterogeneous iridium oxide nanoparticles. Several molecular Ir^{IV} compounds with very similar electronic spectra are also known. For instance, Wilkinson's (III)-(III)-(IV) acetate-trimer[47] or Sykes' (IV)-(IV) hydroxo-dimers[48,49] exhibit strong, broad absorption bands around 580 nm. Importantly, these complexes were obtained via the same general synthetic protocol as Harriman's nanoparticle solutions, but with slight variations in iridium concentration and pH. The hydroxo-dimers also relate to intermediates thought to be involved in IrO_2 formation from hexachloroiridate. Scheme 1 summarizes the aqueous solution chemistry of iridium en route to IrO_2,[48−58] illustrating the importance of concentration and pH as well as the difficulty of interpreting the purple-blue solutions of Ir^{IV} in terms of specific species.

The formation of similar purple-blue solutions has also been observed during water and C−H oxidation catalysis with certain organometallic iridium complexes in the presence of strong chemical oxidants such as CAN (ceric ammonium nitrate, $[NH_4]_2[Ce^{IV}(NO_3)_6]$). This has led to discussions as to whether the true active species in these systems were molecularly defined complexes or IrO_2 nanoparticles generated in situ.[59] Some oxidative degradation pathways of the Cp* ligand in certain complexes have been identified from NMR data,[60,61] and small IrO_2 clusters were detected by electron microscopy in some cases.[8,59] Fukuzumi recently investigated the oxidative stability of a series of Cp*Ir complexes with CAN and found interesting ligand effects in the formation of nanoparticles as observed by TEM and DLS.[62] Furthermore, the aqua complex $[Cp^*Ir(H_2O)_3]^{2+}$ is known to be a good precursor for the controlled anodic deposition of an amorphous iridium oxide material containing a carbon admixture,[63] a highly active and robust heterogeneous water oxidation catalyst that exhibits electrochromism[64] and has a λ_{max} at 580 nm in its oxidized form (the so-called "blue layer", **BL**).[65] Here, we show by DLS that the ca. 580 nm band often seen in the catalytic solutions is not necessarily associated with the formation of iridium oxide particles, and that many of the Cp* precursors previously studied are resistant to particle formation under strongly oxidizing conditions.

dx.doi.org/10.1021/ja3033026 | J. Am. Chem. Soc. 2012, 134, 9785−9795

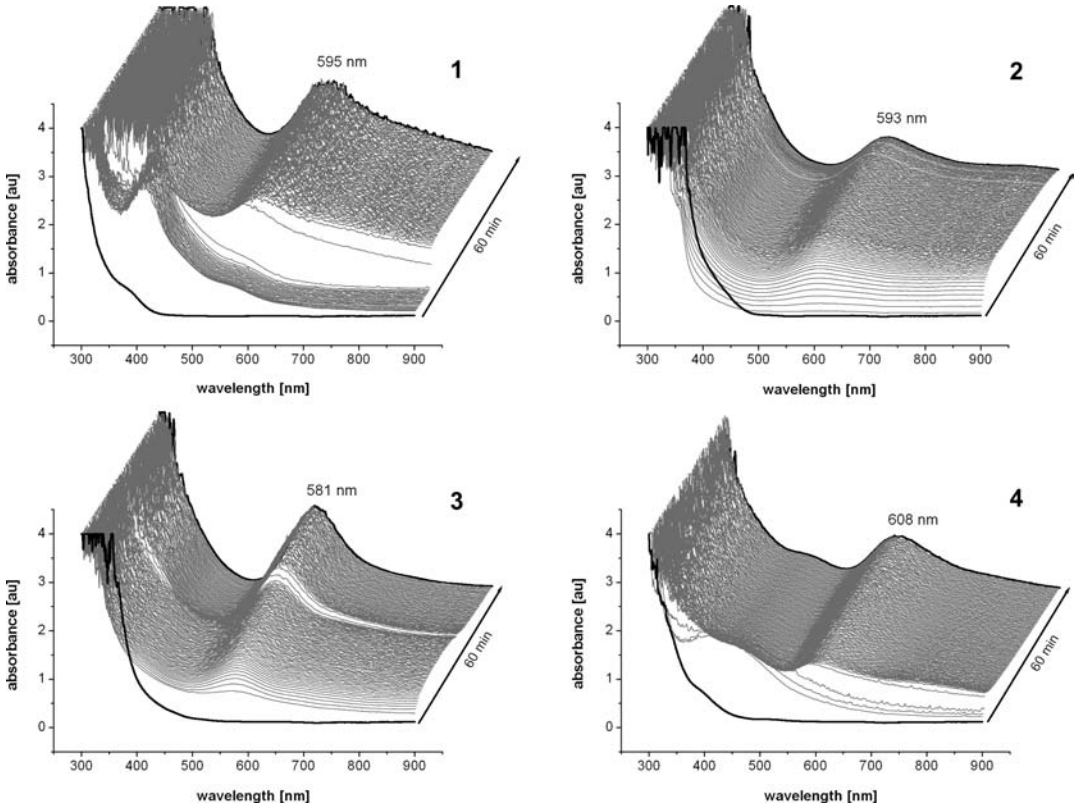

Figure 2. Evolution of UV−vis spectra of complexes **1**−**4** in water (1 mM [Ir]) at room temperature with 100 equiv of $NaIO_4$ added after the first spectrum (30-s intervals, max absorbance 4 au).

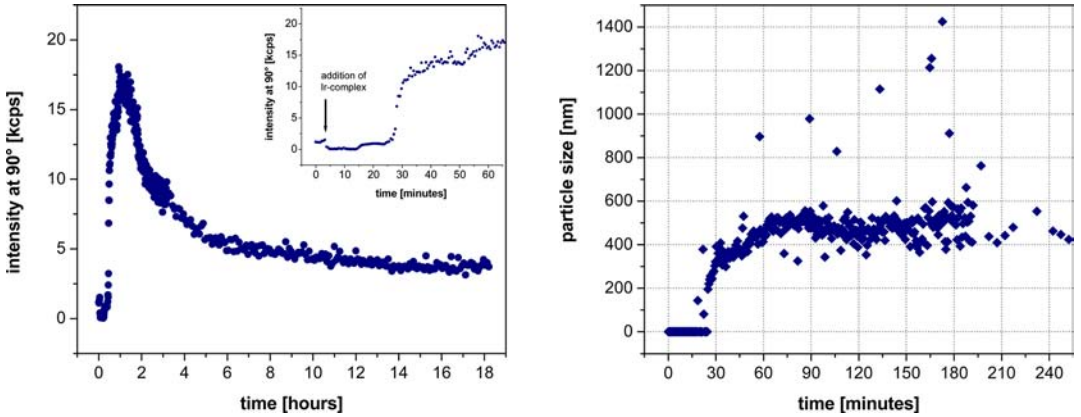

Figure 3. Light scattering intensity and mean particle size of a diffusional mixture of complex **1** (2.5 mM [Ir]) and 100 equiv of $NaIO_4$ in water at room temperature over time (correlation functions and statistics are provided in the Supporting Information).

RESULTS AND DISCUSSION

To examine the connection between the appearance of a ∼580 nm UV band and in situ particle formation during catalysis with chemical oxidants, four representative Cp^*Ir^{III} precursor complexes (Figure 1) were investigated by UV−vis spectroscopy and time-resolved DLS.

The different chelate ligands of complexes **2**−**4** in Figure 1 impart distinct electronic effects as compared to the hydroxo/aqua[66] complex **1**, ranging from the π-acidic 2,2′-bipyridine (bipy) in complex **2** to the more σ-basic 2-phenylpyridine (phepy) in complex **3** to the π-basic 2-(2′-pyridyl)-2-propanolate (pyalc) ligand in complex **4**.[67] Previous studies have shown that Cp*Ir precursors based on these ligands are all similarly active both in water[4] and in C−H[2] oxidation catalysis with CAN. To exclude interference from halides and impart increased water solubility, the corresponding hydroxo complexes were used here instead of the more commonly employed chloro precursors.

We have recently shown that periodate ($NaIO_4$) may serve as alternative chemical oxidant to CAN with a range of catalysts, yielding comparable oxidation efficiencies with negligible contribution from periodate coupling.[68] Unlike the highly acidic and colored CAN which tends to precipitate ceria,[69,70] the use of the colorless and steadily soluble $NaIO_4$ allowed working catalyst solutions to be studied by optical absorption spectroscopy (Figure 2) and light scattering (vide infra).

With periodate, all the observed spectral changes could be exclusively attributed to iridium speciation in solution. As can

dx.doi.org/10.1021/ja3033026 | J. Am. Chem. Soc. 2012, 134, 9785−9795

be seen from Figure 2, complexes **1**−**4** all quickly yielded deep blue solutions with intense, broad absorption bands around 580−610 nm with only slightly different kinetics and λ_{max} values (see also Supporting Information). Similar observations have been made with other Cp*Ir complexes and CAN, and the results have been interpreted as direct evidence for rapid in situ IrO_x formation.[59] However, our EQCN experiments had revealed a marked difference between complexes **1** and **4** under electrochemical conditions where complex **4** did not deposit any heterogeneous material even at potentials up to 1.5 V, but complex **1** readily formed **BL** material on the anode from the first scan.[23]

To investigate whether nanoparticles formed in these solutions along with the appearance of the ∼580 nm UV−vis band, the reaction of complex **1** with 100 equiv of $NaIO_4$ was followed by time-resolved DLS over several hours. Using a laser operating at 532 nm (in the "spectroscopic valley" of Figure 2), well-defined and reproducible scattering profiles were obtained (Figure 3).

Immediately after the iridium complex **1** was injected into the oxidant solution, background scattering intensity dropped slightly due to a slight increase in absorption. Additional data and control experiments ruled out masking of particle formation by absorption (see Supporting Information and below). The slight increase in background intensity after about 10 min reflected the appearance of the blue color (see Figure 2), but the correlation function did not correspond to any particle size for another 10 min (Figure 3, right). After this 20-min lag phase, rapid particle formation set in with swiftly increasing particle sizes. Although our instrumentation can resolve nanometric particle sizes at concentrations as low as 10 ppm, the smallest particles detected at the onset of formation were already 50−100 nm in size, indicating a high initial growth rate. After about 1 h, the particles had reached mean hydrodynamic diameters of ∼500 nm and exhibited maximum scattering intensity. Thereafter, the size distribution showed increasing polydispersity and scattering intensity slowly decreased due to sedimentation of the larger agglomerates (representative size distribution data are provided in the Supporting Information).

When the reaction mixtures were either centrifuged or allowed to stand for several days, a blue-black precipitate separated from the supernatant, which still retained its deep blue color. TEM analysis of the recovered solid confirmed that the large particles of several hundred nanometers size detected by DLS were aggregates consisting of primary particles of about 20 nm diameter (Figure 4). Powder X-ray diffraction showed that the solid was amorphous as recovered but converted to tetragonal IrO_2 after heating to 450 °C in air (see Supporting Information).

Importantly, the lag phase between mixing and particle formation was about twice as long as it took for complex **1** to form its distinct 595 nm UV−vis band under these conditions, meaning that the formation of the deep blue color clearly preceded nanoparticle formation. This suggests that the appearance of a ∼580 nm band cannot be safely equated with the presence of nanoparticles as previously thought. Since significant O_2 evolution occurs with precursor **1** before particle formation is apparent,[4] molecular iridium species must be the catalysts initially active in solution. Injecting a sample of recovered particles into a fresh $NaIO_4$ solution, however, also caused immediate oxygen evolution (see Supporting Information). Thus, both the solution species and the nanoparticles are

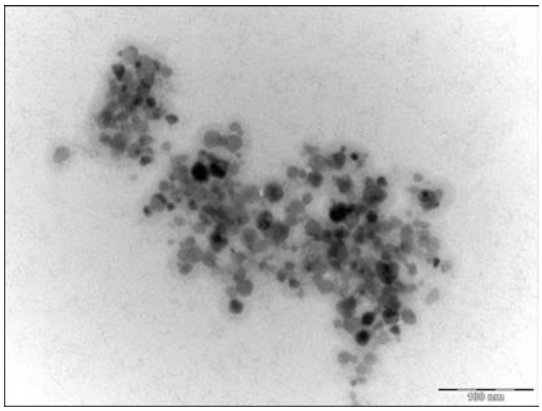

Figure 4. TEM picture of a sample of the precipitate from Figure 3 at 200 000× magnification.

active oxidation catalysts, and only time-resolved DLS experiments, but not UV−vis spectroscopy, allowed both cases to be distinguished in real time.

When the isolated precipitate was thoroughly washed with and resuspended in neutral water with the aid of sonication, colorless suspensions void of any UV−vis feature were obtained that appeared homogeneous to the naked eye, but exhibited intense light scattering (Figure 5). Obviously, the deep blue color caused by the broad ∼580 nm absorption band did not originate from suspended particles in solution. This observation casts further doubt on the automatic identification of particle formation with the ∼580 nm band. When these colorless suspensions of 500-nm sized particles were treated with concd HCl at room temperature, the solution immediately turned deep blue and DLS showed instantaneous dissolution of more than 95% of the particles, as evidenced by an intensity decrease from 90 to 5 kcps (Figure 5). Furthermore, the remaining particle population was reduced to a size of 150 nm. The redissolution of iridium oxides in strong mineral acids, but only when freshly precipitated, has long been known[34] and used historically as a purification procedure.[31−33] Consistent with these reports, we confirmed that anhydrous, crystalline IrO_2 did *not* dissolve in concd HCl and did *not* colorize the solution, as is also the case for other iridium oxides such as our **BL** material,[63,65] IrO_x nanoparticles,[41,44,71] and bulk IrO_2 catalysts.[64,72,73]

The blue supernatant from which the precipitated particles had been isolated could be reduced by addition of ethanol or sulfite to yield bright yellow solutions with a λ_{max} at 350 nm (Figure 6, left) that still would not exhibit any light scattering. The same procedure could be performed with solutions of the recovered particles that had been dissolved in HCl. Figure 6 (right) depicts particle separation and resuspension (A → B), particle dissolution by acid (B → A), and reduction of particle-free blue solutions (A → C).

This behavior is most consistent with molecular Ir^{IV} species giving rise to the distinctive blue color around 580 nm in the UV−vis, and serving as precursors to the heterogeneous oxide material under suitable conditions. The particles themselves appear not to contribute to the color of the solution and their formation is reversible as a function of the pH. Furthermore, the blue Ir^{IV} solution species may be easily reduced to a yellow species, all consistent with the earlier proposals of Richens and Sykes (see Scheme 1).[49] Although our conclusions only strictly apply to the systems studied here, the data do raise questions

dx.doi.org/10.1021/ja3033026 | J. Am. Chem. Soc. 2012, 134, 9785−9795

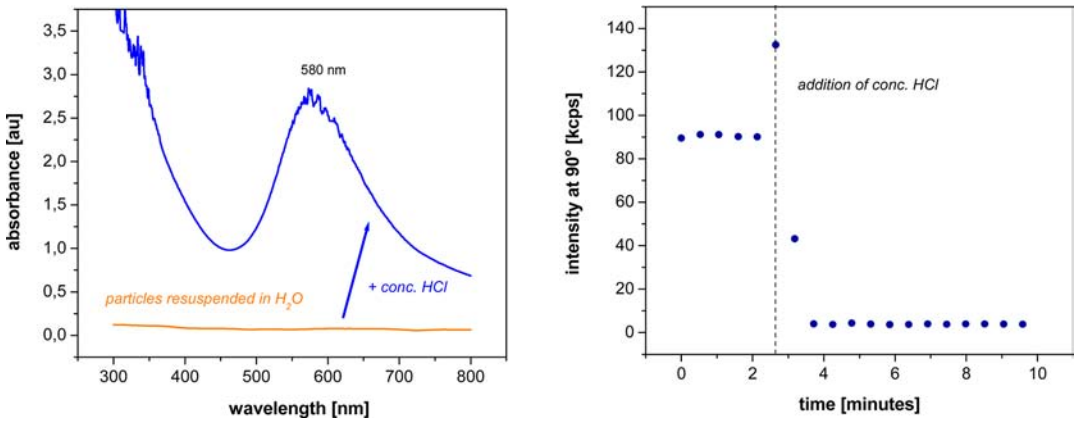

Figure 5. UV−vis spectra (left) and light scattering intensity (right) of the recovered precipitate resuspended in neat water upon treating with concd HCl at RT.

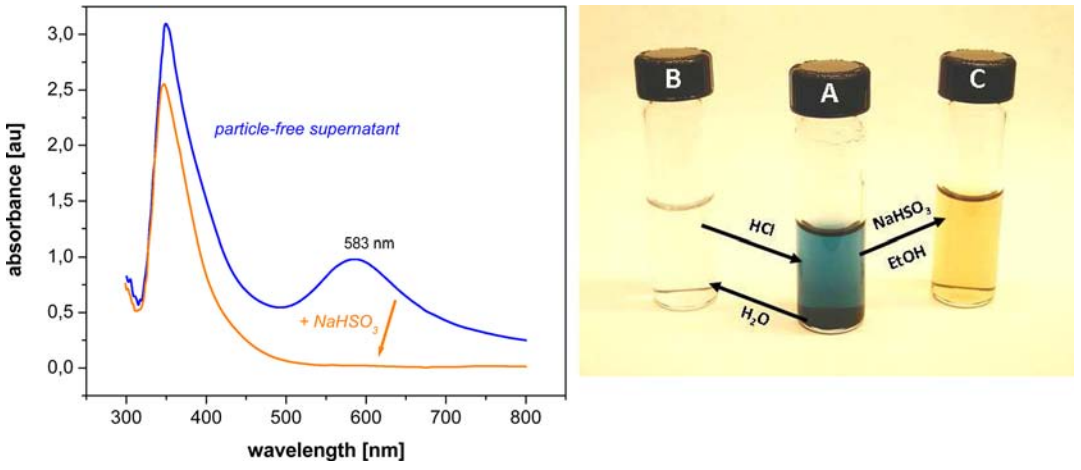

Figure 6. UV−vis spectra of particle-free blue solution upon reduction (left) and a photograph of samples illustrating the interconversion of blue solution (A, no light scattering by the supernatant), colorless particle suspension (B, strong light scattering), and reduced yellow solution (C, no light scattering).

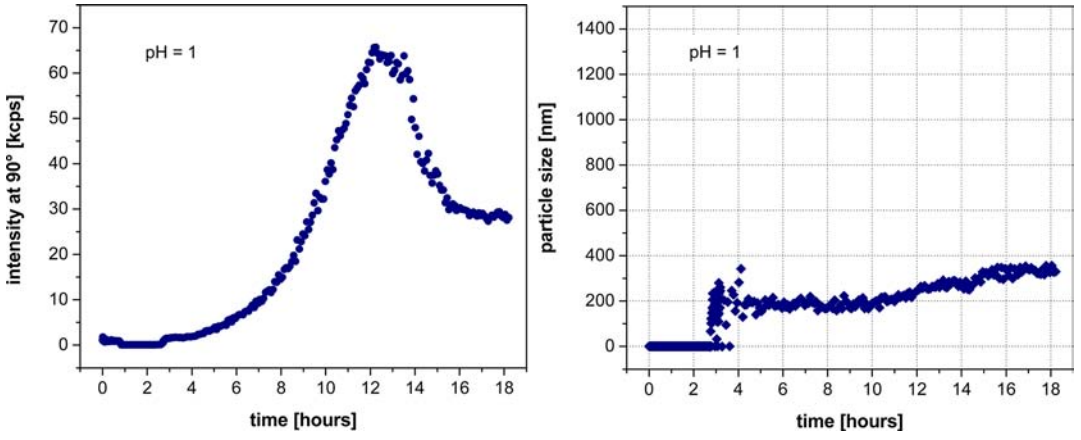

Figure 7. Light scattering intensity and mean particle size of a diffusional mixture of complex **1** (2.5 mM [Ir]) and 100 equiv of $NaIO_4$ in water at pH 1 with H_2SO_4 at room temperature over time.

that could well apply more generally to oxidation catalysis with molecular iridium precursors.

When water oxidation using complex **1** with 100 equiv of $NaIO_4$ as in Figure 3 was performed at pH 1 (H_2SO_4), particle formation was greatly delayed (Figure 7, left). In this case, the lag phase before the onset of particle formation was nearly 3 h and the growth rate was much slower with maximum scattering intensity being reached only after 13 h. Near-monodisperse particles measuring 200−300 nm in diameter formed in this case (Figure 7, right).

This finding has implications for applying oxidation catalysis with soluble iridium complexes. As the oxidation of H_2O to O_2 liberates protons as byproduct, the reaction automatically leads to a decrease in pH that would progressively disfavor particle

dx.doi.org/10.1021/ja3033026 | J. Am. Chem. Soc. 2012, 134, 9785−9795

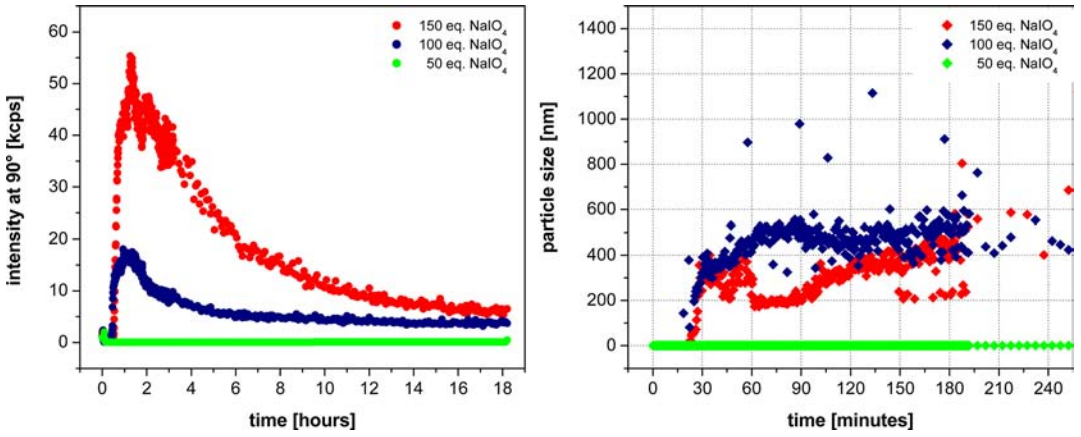

Figure 8. Light scattering intensity and mean particle size of a diffusional mixture of complex **1** (2.5 mM [Ir]) and various equivalents of $NaIO_4$ in water at room temperature over time.

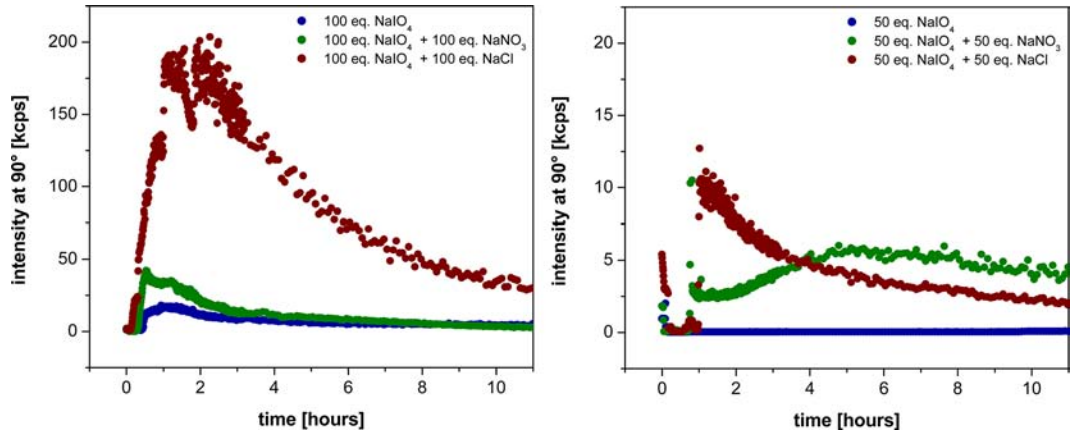

Figure 9. Light scattering intensity of diffusional mixtures of complex **1** (2.5 mM [Ir]) with various amounts of $NaIO_4$ and NaCl or $NaNO_3$ in water at room temperature over time.

formation when working in a closed, unbuffered system. This effect was demonstrated in a separate experiment where a small amount of preformed nanoparticles was added to a solution of complex **1** and $NaIO_4$ directly at the time of mixing. As observed by DLS, even in the absence of additional acid the added particles dissolved in the reaction mixture within seconds (as in Figure 5, right), and the subsequent particle formation profile proceeded unaffected by the inoculation procedure. Monitoring the pH of a mixture of complex **1** and 100 equiv of $NaIO_4$ over time indeed showed a sharp decrease in pH due to immediate water oxidation activity (see Supporting Information), plausibly responsible for the dissolution of the added particles.

As is often the case for the reductive formation of metal nanoparticles from organometallic complexes,[74] the production of heterogeneous oxide material from precursor **1** also appeared to be driven by the solution potential. When the number of oxidizing equivalents was varied while keeping the iridium concentration unchanged, different amounts of particles were produced with unchanged dynamics and similar average sizes (Figure 8). In conjunction with the negative inoculation test, this finding is good evidence against autocatalytic nanoparticle formation from the organometallic precursor, and suggests a classical LaMer mechanism[75] of spontaneous nucleation due to supersaturation followed by diffusive growth.

Moving to 150 equiv of $NaIO_4$ from 100 equiv led to a tripling of the maximum scattering intensity after 1 h, but the particle-free lag phase of ~20 min remained unchanged. On the other hand, reducing the loading to 50 equiv of $NaIO_4$ (125 mM) neither resulted in an increase in scattering nor the development of any exponential decay in the correlation functions over the entire course of the DLS experiment (see Supporting Information). The solution still developed its characteristic blue color with an intense λ_{max} at 595 nm within minutes and remained unchanged for weeks. This observation emphasizes that in situ nanoparticle formation crucially depends on the exact reaction conditions, and cannot be judged based on the structure of a precursor complex or the potential of a reagent alone.

The presence of inorganic salts influenced both the dynamics and the extent of oxidative particle formation from complex **1**. When 100 equiv of $NaNO_3$ (0.25 M) were added to an experiment with 100 equiv of $NaIO_4$, the particle-free lag phase was shortened to ~15 min and maximum scattering intensity doubled (Figure 9, left). Adding 100 equiv of NaCl (0.25 M) caused an even shorter lag time of only 5 min and nearly 10 times more particles formed. In both cases, only blue-black solids were recovered after 18 h (no salt co-precipitation), and the supernatant was less intensely colored than in the absence of additional salt, consistent with a greater degree of particle formation from the blue Ir^{IV} solution species. These

dx.doi.org/10.1021/ja3033026 | J. Am. Chem. Soc. 2012, 134, 9785–9795

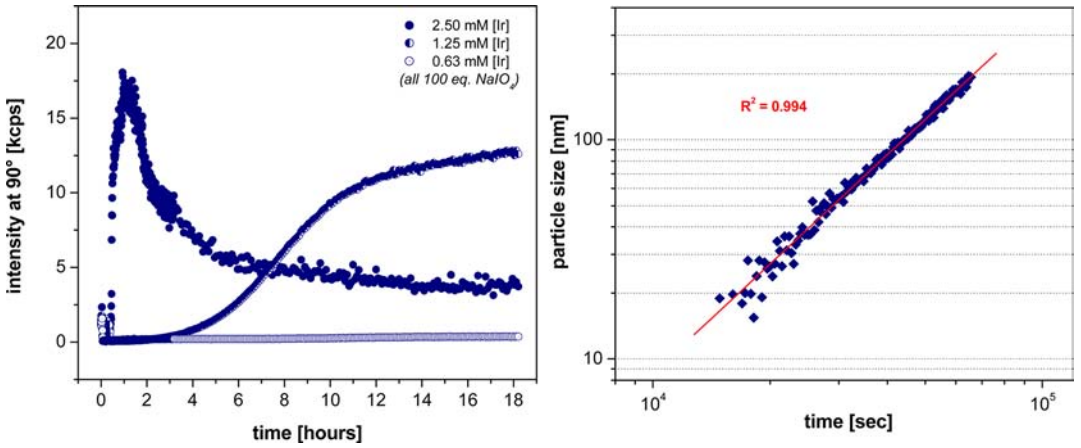

Figure 10. Light scattering intensity of diffusional mixtures of complex **1** and 100 equiv of $NaIO_4$ in water at various concentrations at room temperature over time (left) and log/log plot of mean particle size over time of the run at 1.25 mM iridium concentration (right, including a power-law fit $a = (3.9 \times 10^{-6})t^{1.59}$).

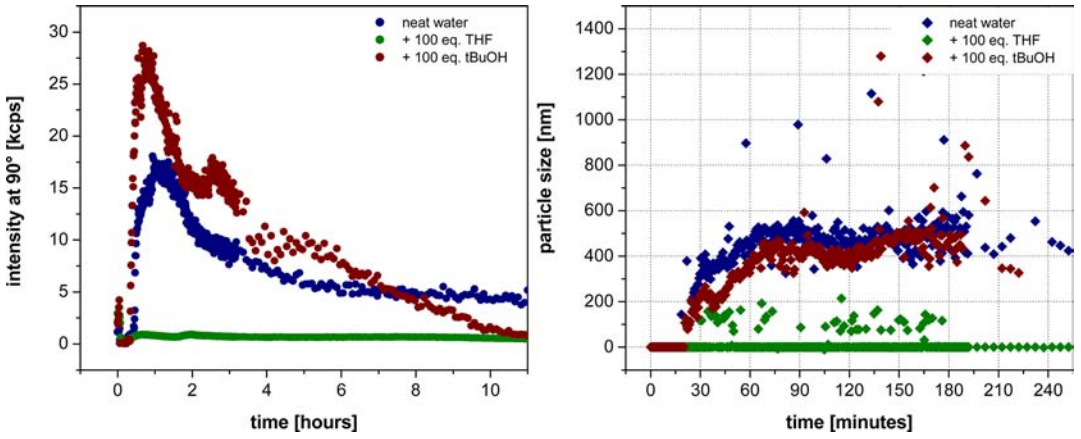

Figure 11. Light scattering intensity and mean particle sizes of a diffusional mixture of complex **1** (2.5 mM [Ir]) and 100 equiv of $NaIO_4$ plus 100 equiv of organic substrate in water at room temperature over time.

observations may have implications for performing oxidation catalysis with Ir-complexes in aqueous buffers as well as electrochemical studies, which are typically conducted in up to 1 M electrolyte solutions. The particle-promoting salt effect was even strong enough to induce particle formation from complex **1** under conditions that did not give any heterogeneous material with the oxidant alone (Figure 9, right). Under these conditions, the initial lag phase was nearly 1 h for both $NaNO_3$ and NaCl, and similar amounts of particles formed at comparable particle sizes.

As expected for an oligomerization reaction, variation in iridium concentration strongly affected the kinetics of particle formation. Figure 10 compares the effects of doubling and quadrupling reagent dilution on particle formation from complex **1** with $NaIO_4$ in the absence of any additives. At half the usual concentration, nanoparticle formation was greatly delayed, showing smooth growth kinetics after about 3 h latency time. After 22 h, the same maximum scattering intensity was seen as with the initial concentration, and precipitation set in (data not shown). Analyzing mean particle sizes in the growth regime over time showed a clean power-law dependence characteristic of a purely diffusion-controlled process (Figure 10, right), meaning that each contact in solution leads to an increase in size at essentially zero activation energy.[76−79] Because of the slower growth rate under more dilute conditions, primary particles of 15−20 nm in diameter were well resolved soon after the onset of particle formation. The size-distribution analysis over time showed that polydispersity progressively increased as the particles grew in size (see Supporting Information).

The slower particle formation under dilute conditions could be used to study the growth mechanism by angular-dependent static light scattering. A log/log plot of the development of relative scattering intensity (I/I_0) as a function of the wave vector (q) showed the development of aggregates over time (see Supporting Information). When the particles had reached their maximum sizes in solution (~30 h), the intensity behaved as $I/I_0 \sim q^{-Df}$ with an exponent of −1.95, indicating a fractal dimension D_f comparable to that expected for diffusion-limited aggregation.[77] The persistence of a peak in I/I_0 at $q \sim 0.0302$ nm^{-1} throughout the experiment indicates a primary particle size of $1/q \sim 33$ nm, suggesting that under the conditions applied particle growth above 30 nm occurred via agglomeration instead of further Ostwald ripening.[74] Considering that additional hydration shells are included in particle sizes derived from light scattering,[27] this value is in excellent agreement with the TEM analysis of the recovered precipitate (Figure 4).

When a reactive organic substrate such as THF was added to complex **1**, the oxidizing power of the solution was effectively diverted to C−H oxidation,[2] and particle formation was greatly

dx.doi.org/10.1021/ja3033026 | J. Am. Chem. Soc. 2012, 134, 9785−9795

reduced (Figure 11). Roughly one order of magnitude less heterogeneous material formed and mean particle sizes remained below 200 nm. This finding of a protective effect of the presence of a reactive substrate such as THF on the stability of the Cp*Ir oxidation catalysts relates to our studies on catalytic oxidation of organic compounds under similar conditions.[2] The addition of an oxidation-resistant organic component such as ^{t}BuOH, however, caused the opposite effect (Figure 11). While initial particles sizes were unaffected by the presence of ^{t}BuOH, the maximum scattering intensity increased to even higher values after a virtually unchanged lag phase of ~20 min. After about 4 h, when scattering intensity started to decrease more rapidly than in neat water, particle sizes increased to very large diameters of up to 30 μm in the presence of ^{t}BuOH. We interpret this behavior as a largely unaffected initial water oxidation activity, followed by particle nucleation and growth as in neat water. The following agglomeration was then promoted by the oxidation-resistant organic co-solvent, leading to complete sedimentation of all suspended nanoparticles after 12 h.

In sharp contrast to complex **1**, with the bipy-ligated precursor **2** and 100 equiv of $NaIO_4$ in neat water, no increase in light scattering intensity was detected over 18 h (Figure 12).

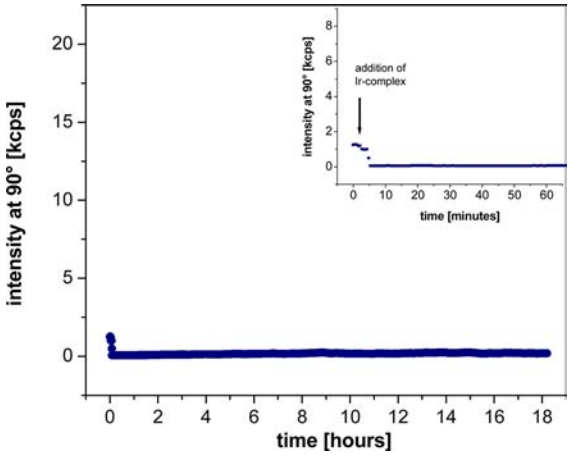

Figure 12. Light scattering intensity of a diffusional mixture of complex **2** (2.5 mM) and 100 equiv $NaIO_4$ in water at room temperature over time.

Even after one week at room temperature, no precipitate could be isolated from the solution. In an attempt to enforce oxidative decomposition and nanoparticle formation, complex **2** was injected into a saturated $NaIO_4$ solution (~0.5 M ≈ 200 equiv), but the DLS profile remained featureless even under these harsh conditions.

This result clearly shows that the chelate ligand can impart a strongly stabilizing effect to the Cp*Ir fragment, which in this case completely prevents oxidative particle formation. As can be seen from Figure 2, precursor **2** did form an intense and broad UV−vis band around 590 nm, but no nanoparticles of any sort were detected. Also, as shown elsewhere,[68] catalytic O_2 evolution occurs from the solution under these and even more dilute conditions. The blue solution could be readily reduced back to yellow (as in the case of the separated supernatant of complex **1** in Figure 6, left) and still showed zero scattering intensity. The high stability of precursor **2** in contrast to the related $[Cp^*Ir(4,4'\text{-bishydroxy-2,2'-bipyridine})(H_2O)]^{2+}$, which was found to decompose readily with CAN,[62] can be attributed to a higher oxidation resistance of unsubstituted bipy as compared to the phenolic 4,4′-bishydroxy-2,2′-bipyridine.[80] Analogous complexes with less activating −OMe, −Me, and −COOH 4,4′-substitutents proved more stable in the same study.[62]

Gratifyingly, precursor **3** did also not form any nanoparticles with up to 200 equiv of $NaIO_4$ in water (Figure 13). This is surprising given that the cyclometalated phepy ligand in complex **3** might have been considered less oxidation-resistant than the bipy ligand in complex **2**.[80]

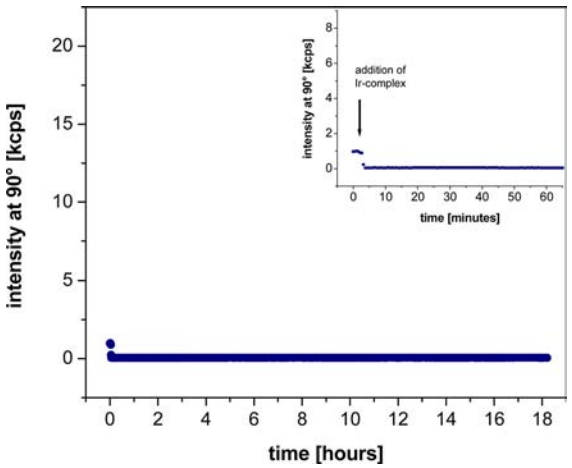

Figure 13. Light scattering intensity of a diffusional mixture of complex **3** (2.5 mM) and ~200 equiv of $NaIO_4$ in water at room temperature over time.

Similarly, precursor **4**, which had already been shown not to deposit any heterogeneous material on the anode during electrode-driven water oxidation catalysis,[23] was also found to be stable toward oxidative nanoparticle formation with $NaIO_4$ (Figure 14). No particle sizes were derivable from the correlation function, and the reaction mixtures remained homogeneous solutions for weeks.

To test if traces of nanoparticles could have been masked by the coloration of the solution, some recovered particles were added to the reaction mixture after the experiment shown in

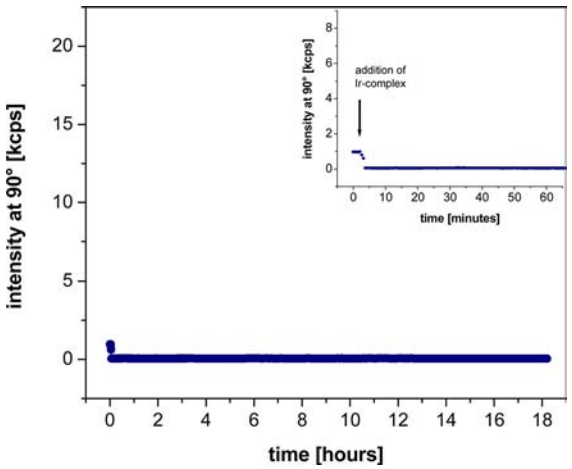

Figure 14. Light scattering intensity of a diffusional mixture of complex **4** (2.5 mM) and ~200 equiv of $NaIO_4$ in water at room temperature over time.

dx.doi.org/10.1021/ja3033026 | J. Am. Chem. Soc. 2012, 134, 9785−9795

Figure 14. Even a very small amount of particles (1% of a previous run) could easily be observed through the deep emerald-blue solution (see Supporting Information), suggesting that no solid had escaped the analysis. The reaction of complex **4** with $NaIO_4$ was also followed by DLS at pH 1 (H_2SO_4) in order to test whether the basic pyalc ligand would dissociate from the metal under highly acidic conditions, but no particles could be detected in this experiment either.

These results strongly suggest that oxidation catalysis with complexes **2**–**4** is truly homogeneous in nature over a wide range of conditions with $NaIO_4$. It is interesting that a variety of chelate ligands appear to be effective in stabilizing Cp^*Ir^{III} precursors from nanoparticle formation. The molecular identity of the blue resting state[81,82] and that of the the active catalyst species, including the question of whether the Cp* ligand is retained, are all currently under investigation.

■ CONCLUSION

We have shown that time-resolved dynamic light scattering can be used as a noninvasive in operando technique to distinguish homogeneous from heterogeneous oxidation catalysis in real time. In conjunction with UV–vis reaction profiles, we were able to make clear that the appearance of ∼590 nm UV–vis bands is not a reliable indicator of nanoparticle formation during catalysis with molecular iridium precursors and chemical oxidants such as sodium periodate. We found that $[Cp^*_2Ir_2(\mu\text{-}OH)_3]OH$ formed amorphous oxide nanoparticles with lag phases ranging from 5 min to 3 h after being injected into periodate solutions at room temperature. While the dynamics of nanoparticle formation depended mostly on iridium concentration and pH, the amount formed and the growth rate appeared to be governed by the solution potential and the presence of inorganic salts or organic co-solvents (a summarizing table can be found in the Supporting Information). Nucleation is believed to be reaction-controlled, but growth above 30 nm in diameter proceeded via diffusion-limited agglomeration. Various chelate ligands such as 2,2′-bipyridine, 2-phenylpyridine, or 2-(2′-pyridyl)-2-propanolate were effective in preventing nanoparticle formation, and the corresponding complexes are thus believed to be truly homogeneous oxidation catalysts. The ligand effect is also manifested in slightly different λ_{max} values of the blue reaction mixtures, so the chelate ligands do not seem to be entirely lost at this stage. The data obtained are expected to be important for the successful development of selective, homogeneous C–H oxidation catalysts as well as for the implementation of photoelectrochemical cells for light-driven water splitting.

■ EXPERIMENTAL SECTION

General. Organic solvents of commercial grade were purified by passing over activated alumina with dry N_2. Deionized water was supplied from a centralized purification system (Dept. of Chemistry, Yale University). All chemicals were purchased from major commercial suppliers and used as received. 2-(2′-pyridyl)-2-propanol,[83] [(η^5-pentamethylcyclopentadienyl)Ir(2-phenylpyridine-κC,κN)Cl],[84] and aqueous stock solutions of $[(\eta^5\text{-pentamethylcyclopentadienyl})_2Ir_2(\mu\text{-}OH)_3]OH$[85] (**1**) were prepared following literature procedures, and analytical data were in accordance with the reported values. Syntheses were performed under inert atmosphere using Schlenk techniques and analyses were run in air.

Analyses. NMR spectra were recorded at room temperature on either 400 MHz Bruker or 500 MHz Varian spectrometers and referenced to residual protio-solvent signals (δ in ppm). Mass spectrometry measurements were performed by the W. M. Keck Biotechnology Resource Laboratory (Yale University) and elemental analyses by Robertson Microlit Laboratories (Ledgewood, NJ). UV–vis spectra were recorded on a Varian Cary 50 using 1.0 cm quartz cuvettes. Transmission electron microscopy was performed on vacuum-dried samples on copper microgrids coated with elastic carbon using a Zeiss EM-900 TEM operating at 80 kV and equipped with a SIS Megaview III digital camera.

Light scattering experiments were conducted with a multiangle CGS-5000F goniometer setup (ALV GmbH) equipped with eight individual SO-SIPD optical detectors and a Verdi V2 continuous wave DPSS laser (COHERENT), operating at 532 nm with 300 mW at a limiting diode count of 200 000. DLS measurements were obtained with a fixed detector at 90°. Data were collected in intervals of 30 s for all samples continuously over the first 3 h and with a waiting time of 5 min between measurements thereafter. On-board correlator cards provided the scattered light intensity correlation functions $g(\tau)$, which were fit to a second-order exponential decay function to obtain average particle sizes (cumulant analysis). CONTIN analysis[86] was used to obtain particle size distributions (see Supporting Information). For static light scattering (SLS) measurements, the normalized scattered light intensity I/I_0 was obtained simultaneously by all eight detectors over an angular range of 10–150°, corresponding to wave vectors $0.0046 < q < 0.0305$ nm^{-1} (see Supporting Information).

In a typical experiment, the desired amount of oxidant was dissolved in 3 mL of water in air and potential additives (salts or acid) were added. After dissolution of all solids, the solution was passed through a hydrophobic syringe filter (Teflon, 0.2 μm pore size) into the sample vial inside the scattering chamber thermostatted to 22 °C in a toluene bath. New cylindrical screw-cap glass vials (15 × 45 mm) were used for each experiment. The automated measurement was started, and after collection of a few data points, the desired amount of catalyst dissolved in 1 mL of water was added via syringe to start the reaction. The diffusional mixture was left for the analysis in a dark, undisturbed room.

*[(η^5-Pentamethylcyclopentadienyl)Ir(2,2′-bipyridyl)OH] BF_4 (**2**).* This known compound[87] was prepared via an alternative route. Solid 2,2′-bipyridine·HBF_4 (49 mg, 0.2 mmol; obtained as precipitate from 2,2′-bipyridine and HBF_4·OEt_2 in chloroform) was added to an aqueous solution of **1** (0.1 mmol in 5 mL) and the mixture stirred for 16 h at room temperature during which the pale yellow coloration of the solution intensified. Evaporation of solvent yielded a yellow-orange powder which was dried further in vacuo. Yield 114 mg (97%). ^{1}H NMR (400 MHz, D_2O): δ = 8.86 (d, J = 5.5 Hz, 2H), 8.36 (d, J = 8.0 Hz, 2H), 8.12 (t, J = 8.0 Hz, 2H), 7.69 (t, J = 5.5 Hz, 2H), 1.51 (s, 15H). ^{13}C NMR (126 MHz, D_2O): δ = 156.0, 151.4, 140.8, 129.1, 124.2, 87.6, 7.9.

*[(η^5-Pentamethylcyclopentadienyl)Ir(2-phenylpyridine-κC,κN)OH] (**3**).* Solid [(η^5-pentamethylcyclopentadienyl)Ir(2-phenylpyridine-κC,κN)Cl] (103 mg, 0.2 mmol) and Ag_2O (46 mg, 0.2 mmol) were combined in THF (9 mL) and water was added (1 mL). The mixture was stirred in the dark for 24 h at room temperature. Filtration through a 0.2 μm Teflon filter yielded a deep yellow solution, which was carefully taken to dryness under reduced pressure. The pale orange solid was dried in vacuo during which its color darkened. Pentane was added (3 mL) and the suspension was sonicated for 2 min. After the fine solid had settled, the pale yellow supernatant was removed with a pipet and the dark orange powder wasdried in vacuo. Yield 90 mg (90%).^{1}H NMR (400 MHz, CD_2Cl_2): δ = 8.75 (d, J = 5.7 Hz, 1H), 7.85 and 7.71 (m, 2 × 2H), 7.18 (td, J^t = 7.3 Hz, J^d =1.3 Hz, 1H), 7.13 (ddd, J = 7.3 Hz, 5.7 Hz, 1.3 Hz, 1H), 7.07 (td, J^t = 7.7 Hz, J^d =1.3 Hz, 1H), 1.67 (s, 15H). ^{13}C NMR (126 MHz, CD_2Cl_2): δ = 167.4, 165.0, 151.4, 145.7, 137.4, 135.9, 130.8, 124.2, 122.9, 122.5, 119.2, 87.2, 8.9. ESI(+)MS calcd for $C_{21}H_{23}IrN^+$: 480.143, 482.145. Found: m/z = 480.09, 482.09. Anal. Calcd for $C_{21}H_{24}IrNO$: C, 50.58; H, 4.85; N, 2.81. Found: C, 50.84; H, 4.63; N, 2.91.

*[(η^5-Pentamethylcyclopentadienyl)Ir(2-(2′-pyridyl)-2-propanolate-κO,κN)OH] (**4**).* Solid 2-(2′-pyridyl)-2-propanol (27 mg, 0.2 mmol) was added to an aqueous solution of **1** (0.1 mmol in 5 mL) and the mixture stirred for 16 h at room temperature, during which the solution changed from pale yellow to orange. Evaporation of solvent

dx.doi.org/10.1021/ja3033026 | J. Am. Chem. Soc. 2012, 134, 9785–9795

yielded a yellow-greenish powder which was dried further in vacuo. Yield 93 mg (97%). ^{1}H NMR (400 MHz, CD_2Cl_2): δ = 8.63 (d, J = 4.7 Hz, 1H), 7.72 (t, J = 7.5 Hz, 1H), 7.21 (m, 2H), 1.63 (s, 15H), 1.40 (bs, 6H). ^{13}C NMR (126 MHz, CD_2Cl_2): δ = 176.1, 149.7, 137.9, 124.0, 121.4, 82.9, 82.5, 33.1, 9.1. ESI(+)MS calcd for $C_{18}H_{25}IrNO^+$: 462.153, 464.156. Found: m/z = 462.15, 464.15. Anal. Calcd for $C_{18}H_{26}IrNO_2$: C, 44.98; H, 5.45; N, 2.91. Found: C, 45.30; H, 4.94; N, 2.89.

Ten millimolar aqueous catalyst stock solutions were prepared in advance on a 0.1 mmol scale and passed through 0.2 μm pore size Teflon filters. Complexes **1**, **2**, and **4** were sufficiently hydrophilic to dissolve in neutral water giving basic solutions (**1**, pH 11; **2**, pH 9; **4**, pH 10), whereas complex **3** required protonation (pH 3 with H_2SO_4).

■ ASSOCIATED CONTENT

Supporting Information

DLS summary table, UV−vis absorption plots, light scattering raw data, methods of size correlation, particle size distributions, additional test experiments, powder XRD analysis of recovered nanoparticles, water oxidation activity assay, pH time-course plots, static light scattering data. This material is available free of charge via the Internet at http://pubs.acs.org.

■ AUTHOR INFORMATION

Corresponding Author

menachem.elimelech@yale.edu; robert.crabtree@yale.edu

Notes

The authors declare no competing financial interest.

■ ACKNOWLEDGMENTS

This work was supported by the Alexander von Humboldt Foundation (Feodor Lynen Research Fellowship to U.H., supplemented by a grant from the Yale Institute for Nanoscience and Quantum Engineering; synthesis) and the Center for Catalytic Hydrocarbon Functionalization, an Energy Frontier Research Center funded by the U.S. Department of Energy, Office of Science, Office of Basic Energy Sciences under Award Number DE-SC0001298 (catalysis and physical measurements). We thank Barry Piekos for TEM measurements, Alexander R. Parent for O_2 detection experiments, Nathan D. Schley for XRD measurements, and James D. Blakemore, Gary W. Brudvig (all Yale University), and Marc Zimmer (Connecticut College) for valuable discussions.

■ REFERENCES

(1) Zhou, M.; Schley, N. D.; Crabtree, R. H. *J. Am. Chem. Soc.* **2010**, *132*, 12550.
(2) Zhou, M.; Balcells, D.; Parent, A. R.; Crabtree, R. H.; Eisenstein, O. *ACS Catal.* **2012**, *2*, 208.
(3) Hull, J. F.; Balcells, D.; Blakemore, J. D.; Incarvito, C. D.; Eisenstein, O.; Brudvig, G. W.; Crabtree, R. H. *J. Am. Chem. Soc.* **2009**, *131*, 8730.
(4) Blakemore, J. D.; Schley, N. D.; Balcells, D.; Hull, J. F.; Olack, G. W.; Incarvito, C. D.; Eisenstein, O.; Brudvig, G. W.; Crabtree, R. H. *J. Am. Chem. Soc.* **2010**, *132*, 16017.
(5) Lalrempuia, R.; McDaniel, N. D.; Müller-Bunz, H.; Bernhard, S.; Albrecht, M. *Angew. Chem., Int. Ed.* **2010**, *49*, 9765.
(6) Savini, A.; Bellachioma, G.; Ciancaleoni, G.; Zuccaccia, C.; Zuccaccia, D.; Macchioni, A. *Chem. Commun.* **2010**, *46*, 9218.
(7) Hetterscheid, D. G. H.; Reek, J. N. H. *Chem. Commun.* **2011**, *47*, 2712.
(8) Marquet, N.; Gärtner, F.; Losse, S.; Pohl, M.-M.; Junge, H.; Beller, M. *ChemSusChem* **2011**, *4*, 1598.
(9) Meyer, T. J. *Acc. Chem. Res.* **1989**, *22*, 163.
(10) Lewis, N. S.; Nocera, D. G. *Proc. Natl. Acad. Sci. U.S.A.* **2006**, *103*, 15729.
(11) Eisenberg, R.; Gray, H. B. *Inorg. Chem.* **2008**, *47*, 1697.
(12) Crabtree, R. H. *Energy Production and Storage—Inorganic Chemistry Strategies for a Warming World*; John Wiley & Sons: Hoboken, 2010.
(13) Shilov, A. E.; Shteinman, A. A. *Coord. Chem. Rev.* **1977**, *24*, 97.
(14) Crabtree, R. H. *Chem. Rev.* **1985**, *85*, 245.
(15) Labinger, J. A.; Bercaw, J. E. *Nature* **2002**, *417*, 507.
(16) Gunay, A.; Theopold, K. H. *Chem. Rev.* **2010**, *110*, 1060.
(17) Chen, M. S.; White, M. C. *Science* **2007**, *318*, 783.
(18) Que, L.; Tolman, W. B. *Nature* **2008**, *455*, 333.
(19) Zhou, M.; Crabtree, R. H. *Chem. Soc. Rev.* **2011**, *40*, 1875.
(20) Crabtree, R. H. *Chem. Rev.* **2012**, *112*, 1536.
(21) Widegren, J. A.; Finke, R. G. *J. Mol. Catal A: Chem.* **2003**, *198*, 317.
(22) Stracke, J. J.; Finke, R. G. *J. Am. Chem. Soc.* **2011**, *133*, 14872.
(23) Schley, N. D.; Blakemore, J. D.; Subbaiyan, N. K.; Incarvito, C. D.; D'Souza, F.; Crabtree, R. H.; Brudvig, G. W. *J. Am. Chem. Soc.* **2011**, *133*, 10473.
(24) Elimelech, M.; Gregory, J.; Jia, X.; Williams, R. A. *Particle Deposition & Aggregation: Measurement, Modelling and Simulation*, 1st ed.; Butterworth-Heinemann: Boston, MA, 1995.
(25) van de Hulst, H. C. *Light Scattering by Small Particles*, 2nd ed.; Dover: Mineola, NY, 1981.
(26) Bohren, C. F.; Huffman, D. R. *Absorption and Scattering of Light by Small Particles*, 1st ed.; John Wiley & Sons: New York, 1998.
(27) Berne, B. J.; Pecora, R. *Dynamic Light Scattering (With Applications to Chemistry, Biology, and Physics)*, 2nd ed.; Dover: Mineola,NY, 2000.
(28) Trasatti, S. *J. Electroanal. Chem. Interfacial Electrochem.* **1980**, *111*, 125.
(29) Harriman, A.; Pickering, I. J.; Thomas, J. M.; Christensen, P. A. *J. Chem. Soc., Faraday Trans.* **1988**, *84*, 2795.
(30) Mills, A.; Russell, T. *J. Chem. Soc., Faraday Trans.* **1991**, *87*, 1245.
(31) Vauquelin, L. N. *Ann. Chim.* **1814**, *89 & 90*, 150.
(32) Claus, C. *J. Prakt. Chem.* **1846**, *39*, 88.
(33) Claus, C. *J. Prakt. Chem.* **1860**, *80*, 282.
(34) Wöhler, L.; Witzmann, W. *Z. Anorg. Chem.* **1908**, *57*, 323.
(35) Harriman, A.; Thomas, J. M.; Millward, G. R. *New J. Chem.* **1987**, *11*, 757.
(36) Nahor, G. S.; Hapiot, P.; Neta, P.; Harriman, A. *J. Phys. Chem.* **1991**, *95*, 616.
(37) Hara, M.; Waraksa, C. C.; Lean, J. T.; Lewis, B. A.; Mallouk, T. E. *J. Phys. Chem. A* **2000**, *104*, 5275.
(38) Reetz, M. T.; Schulenburg, H. WO2005095671, 2005.
(39) Yagi, M.; Tomita, E.; Sakita, S.; Kuwabara, T.; Nagai, K. *J. Phys. Chem. B* **2005**, *109*, 21489.
(40) Hoertz, P. G.; Kim, Y.-I.; Youngblood, W. J.; Mallouk, T. E. *J. Phys. Chem. B* **2007**, *111*, 6845.
(41) Nakagawa, T.; Beasley, C. A.; Murray, R. W. *J. Phys. Chem. C* **2009**, *113*, 12958.
(42) Nakagawa, T.; Bjorge, N. S.; Murray, R. W. *J. Am. Chem. Soc.* **2009**, *131*, 15578.
(43) Gambardella, A. A.; Bjorge, N. S.; Alspaugh, V. K.; Murray, R. W. *J. Phys. Chem. C* **2011**, *115*, 21659.
(44) Zhao, Y.; Hernandez-Pagan, E. A.; Vargas-Barbosa, N. M.; Dysart, J. L.; Mallouk, T. E. *J. Phys. Chem. Lett.* **2011**, *2*, 402.
(45) Frame, F. A.; Townsend, T. K.; Chamousis, R. L.; Sabio, E. M.; Dittrich, T.; Browning, N. D.; Osterloh, F. E. *J. Am. Chem. Soc.* **2011**, *133*, 7264.
(46) Goel, A. K.; Skorinko, G.; Pollak, F. H. *Phys. Rev. B* **1981**, *24*, 7342.
(47) Uemura, S.; Spencer, A.; Wilkinson, G. *J. Chem. Soc., Dalton Trans.* **1973**, 2565.
(48) Castillo-Blum, S. E.; Richens, D. T.; Sykes, A. G. *J. Chem. Soc., Chem. Commun.* **1986**, 1120.

(49) Castillo-Blum, S. E.; Richens, D. T.; Sykes, A. G. *Inorg. Chem.* **1989**, *28*, 954.
(50) Desideri, P.; Pantani, F. *Ric. Sci.* **1961**, *1*, 265.
(51) Van Loon, G.; Page, J. A. *Can. J. Chem.* **1966**, *44*, 515.
(52) Fine, D. A. *Inorg. Chem.* **1969**, *8*, 1014.
(53) Beutler, P.; Gamsjäger, H. *J. Chem. Soc., Chem. Commun.* **1976**, 554.
(54) Beutler, P.; Gamsjäger, H.; Närtschi, P. *Chimia* **1978**, *32*, 163.
(55) Gamsjäger, H.; Beutler, P. *J. Chem. Soc., Dalton Trans.* **1979**, 1415.
(56) Castillo-Blum, S. E.; Sykes, A. G.; Gamsjäger, H. *Polyhedron* **1987**, *6*, 101.
(57) Rodgers, K. R.; Gamsjäger, H.; Murmann, R. K. *Inorg. Chem.* **1989**, *28*, 379.
(58) Kölle, U. *Coord. Chem. Rev.* **1994**, *135*−*136*, 623.
(59) Grotjahn, D. B.; Brown, D. B.; Martin, J. K.; Marelius, D. C.; Abadjian, M.-C.; Tran, H. N.; Kalyuzhny, G.; Vecchio, K. S.; Specht, Z. G.; Cortes-Llamas, S. A.; Miranda-Soto, V.; van Niekerk, C.; Moore, C. E.; Rheingold, A. L. *J. Am. Chem. Soc.* **2011**, *133*, 19024.
(60) Park-Gehrke, L. S.; Freudenthal, J.; Kaminsky, W.; DiPasquale, A. G.; Mayer, J. M. *Dalton Trans.* **2009**, 1972.
(61) Savini, A.; Belanzoni, P.; Bellachioma, G.; Zuccaccia, C.; Zuccaccia, D.; Macchioni, A. *Green Chem.* **2011**, *13*, 3360.
(62) Hong, D.; Murakami, M.; Yamada, Y.; Fukuzumi, S. *Energy Environ. Sci.* **2012**, *5*, 5708.
(63) Blakemore, J. D.; Schley, N. D.; Olack, G. W.; Incarvito, C. D.; Brudvig, G. W.; Crabtree, R. H. *Chem. Sci.* **2011**, *2*, 94.
(64) Burke, L. D.; Scannell, R. A. *Platinum Met. Rev.* **1984**, *28*, 56.
(65) Blakemore, J. D.; Schley, N. D.; Kushner-Lenhoff, M. N.; Winter, A. M.; D'Souza, F.; Crabtree, R. H.; Brudvig, G. W. *Inorg. Chem.* **2012**, submitted for publication.
(66) Note, upon protonation, **1** readily splits into $[Cp^*Ir(H_2O)_3]^{2+}$ monomers.
(67) Crabtree, R. H. *The Organometallic Chemistry of the Transition Metals*, 5th ed.; John Wiley & Sons: Hoboken, NJ, 2009.
(68) Parent, A. R.; Brewster, T. P.; De Wolf, W.; Crabtree, R. H.; Brudvig, G. W. *Inorg. Chem.* **2012**, DOI: 10.1021/ic300154x.
(69) Hayes, S. A.; Yu, P.; O'Keefe, T. J.; O'Keefe, M. J.; Stoffer, J. O. *J. Electrochem. Soc.* **2002**, *149*, C623.
(70) Ho, C.; Yu, J. C.; Kwong, T.; Mak, A. C.; Lai, S. *Chem. Mater.* **2005**, *17*, 4514.
(71) Lee, Y.; Suntivich, J.; May, K. J.; Perry, E. E.; Shao-Horn, Y. *J. Phys. Chem. Lett.* **2012**, *3*, 399.
(72) Comninellis, C.; Vercesi, G. P. *J. Appl. Electrochem.* **1991**, *21*, 136.
(73) Ardizzone, S.; Trasatti, S. *Adv. Colloid Interface Sci.* **1996**, *64*, 173.
(74) Astruc, D. *Nanoparticles and Catalysis*, 1st ed.; Wiley-VCH: Weinheim, 2008.
(75) LaMer, V. K.; Dinegar, R. H. *J. Am. Chem. Soc.* **1950**, *72*, 4847.
(76) Weitz, D. A.; Huang, J. S.; Lin, M. Y.; Sung, J. *Phys. Rev. Lett.* **1984**, *53*, 1657.
(77) Lin, M. Y.; Lindsay, H. M.; Weitz, D. A.; Ball, R. C.; Klein, R.; Meakin, P. *Nature* **1989**, *339*, 360.
(78) Lin, M. Y.; Lindsay, H. M.; Weitz, D. A.; Klein, R.; Ball, R. C.; Meakin, P. *J. Phys.: Condens. Matter* **1990**, *2*, 3093.
(79) Petsev, D. N.; Chen, K.; Gliko, O.; Vekilov, P. G. *Proc. Natl. Acad. Sci. U.S.A.* **2003**, *100*, 792.
(80) Collins, T. J. *Acc. Chem. Res.* **1994**, *27*, 279.
(81) A Cp^*Ir^{IV} compound has been characterized electrochemically and spectroscopically,[82] however, due to its limited lifetime and dominant absorptions of the oxidant $[Ru^{III}(bipy)_3]^{3+}$, the UV−vis spectrum of the Ir^{IV} species was not accessible.
(82) Brewster, T. P.; Blakemore, J. D.; Schley, N. D.; Incarvito, C. D.; Hazari, N.; Brudvig, G. W.; Crabtree, R. H. *Organometallics* **2011**, *30*, 965.
(83) Wong, Y.-L.; Yang, Q.; Zhou, Z.-Y.; Lee, H. K.; Mak, T. C. W.; Ng, D. K. P. *New J. Chem.* **2001**, *25*, 353.
(84) Scheeren, C.; Maasarani, F.; Hijazi, A.; Djukic, J.-P.; Pfeffer, M.; Zaric, S. D.; Le Goff, X.-F.; Ricard, L. *Organometallics* **2007**, *26*, 3336.
(85) Nutton, A.; Bailey, P. M.; Maitlis, P. M. *J. Chem. Soc., Dalton Trans.* **1981**, 1997.
(86) Provencher, S. W. *Comput. Phys. Commun.* **1982**, *27*, 229.
(87) Ogo, S.; Makihara, N.; Kaneko, Y.; Watanabe, Y. *Organometallics* **2001**, *20*, 4903.